AIAA JOURNAL
Vol. 42, No. 11, November 2004

Wake of a Compressor Cascade with Tip Gap, Part 1: Mean Flow and Turbulence Structure

Chittiappa Muthanna* and William J. Devenport†
Virginia Polytechnic Institute and State University, Blacksburg, Virginia 24061

The purpose of this work is to understand the structure of the vortex-dominated endwall flows found in aircraft engine fans and compressors. Our approach is to model the flow using a linear cascade where detailed turbulence measurements can be made and the relative motion between blade tip and casing can be simulated. The cascade consists of eight 4% thick modified circular-arc blades and operates at a chord Reynolds number of 3.88×10^5 with a thin inlet boundary layer and 12.5 deg of turning. We present baseline results for the tip-leakage flow with stationary endwall. Three component velocity and turbulence measurements are used to reveal the evolution of the flow as a function of distance downstream of the blades for a tip gap of 1.6% chord and as a function of tip gap from 0.8 to 3.3%. Overall, these measurements reveal much of the structure of a tip-leakage vortex wake, the manner of its decay and mechanisms of turbulence production, and its relationship to the two-dimensional parts of the blade wakes. Although the vortex is a region of coherent rotating motion, we find that its dynamics are dominated by the streamwise mean-velocity deficit it produces. Mean velocities associated with the deficit are more than twice as strong as those associated with the rotating motion and decay more slowly with downstream distance. Turbulence kinetic energy in the vortex is produced almost entirely by velocity gradients associated with the deficit. Turbulent activity is thus centered in an arc-shaped region above the vortex center where these gradients are large.

Introduction

CONSIDER the flow through a high-bypass-ratio aircraft jet engine. Air flowing into the engine first encounters a large fan with blades that shed a set of wakes into the flow. Near the engine casing, tip-leakage vortices formed by the interaction of the fan-blade tips and casing boundary layer are also formed. These vortices, the casing boundary layer, and the outer parts of the wakes continue through the engine bypass where they impinge on a set of stator vanes. This interaction is important not only because it influences the aerodynamic efficiency of the engine, but also because it generates noise.

Accurate predictions of the mean flowfield entering the stator are required for aerodynamic and tone-noise calculations. Estimates of the turbulence field and space–time correlations are required for broadband noise calculations. These predictions require detailed understanding of the mean flow and turbulence structure downstream of the fan. This understanding is particularly important because of the long distances involved. The axial separation between fan and stator can be as large as four axial tip chord lengths. The flow, evolving along a helical path, can cover a distance of more than twice this between fan and stator. To calculate the evolution of the mean flow over this distance requires detailed calibration of a turbulence model, supported by understanding of the turbulence stress fields, of the balance of turbulence kinetic energy, and of the main turbulence-energy-generating mechanisms. An understanding of the eddy structure contained within the turbulence is required to determine the space–time correlations needed for broadband noise calculations.

The flow near the casing is perhaps the least understood part of the fan wake. This is not to say that the formation of tip-leakage vortices and the flows associated with them have not been researched. Indeed, tip-leakage flows have been the subject of intensive research for at least the past 30 years. Particularly relevant here are the studies that have been performed on compressor rotors, linear cascades, and in axial propulsion pumps.

During the 1980s and 1990s, Lakshminarayana and coworkers (see Refs. 1–16) carried out a series of experiments at Pennsylvania State University (Penn State) on a compressor rotor with inlet guide vanes, a design pressure rise coefficient of 0.49, a tip turning of 16 deg, and an 18%-chord thick casing inlet boundary layer. Studies were made for tip gaps between 1 and 3.4% of the tip chord and for operating conditions at, above,[9,11] and below[7,8] design loading. Measurements were made within the rotor and immediately downstream. These reveal the leakage flow originating from the suction side of the tip between the 25 and 50%-chord locations and streaming out across the casing to form a low-momentum region near center passage.[3,5,10,13] Toward the trailing edge the low-momentum region moves further toward the pressure side of the passage and grows, extending about 15% of tip chord away from the endwall.[2,3,10,15] Turbulence levels in the low-momentum region are high and grow with distance downstream.[4] Turbulence spectra in this region show a broadband turbulent form, and radial turbulence intensities exceed axial and tangential ones—an imbalance attributed to centrifugal effects.[4] Downstream of the rotor some of these studies[1,2,5,14,16] report the diffusion of the flow nonuniformities, but the low-momentum region associated with the tip leakage remains clearly distinct at least one chord length downstream of the trailing edge.[13] The flow nonuniformities associated with the tip leakage and their penetration into the blade passage are seen to increase with blade loading,[8,9,11] indicating the importance of the pressure forces that drive the leakage flow through the tip gap.

Except at a larger tip gap of 3.4% chord,[14] the Penn State studies do not reveal the low-momentum region as an organized tip-leakage vortex. This is in contrast to the results of Inoue and coworkers,[17,18] who studied case of a more lightly loaded rotor with downstream stator. Their rotor produced a pressure rise coefficient of 0.4 and a flow turning of 6.7 deg and had a much thinner inlet boundary layer (1 to 1.5% tip chord) and lower inlet turbulence levels (because of the absence of inlet guide vanes). Their mean flow results, measured up to 41% chord downstream of the rotor exit, show clear evidence of a rolled-up leakage vortex for all tip gaps studied (0.4 to 4.6% chord). The vortex is seen as a region of circulating mean crossflow and one of large mean kinetic energy defect. Increasing the tip gap was found to increase the size of the tip-leakage vortex.

Received 17 September 2003; revision received 18 June 2004; accepted for publication 23 June 2004.

*Graduate Assistant, Department of Aerospace and Ocean Engineering, 215 Randolph Hall. Student Member AIAA.

†Professor, Department of Aerospace and Ocean Engineering, 215 Randolph Hall. Senior Member AIAA.

Consistent with a strengthening vortex, increases in tip gap up to 1.7% chord were seen to move the position of the vortex across the casing toward the wake of the pressure-side blade and increase the angle between the path taken by the vortex center and the blade wakes. The streamwise vorticity at the vortex center and its rate of decay with downstream distance were seen to increase with tip gap. Increasing rotor solidity resulted in the vortex crossing the passage and interacting with the wake of the adjacent blade. Pressure and velocity fluctuation measurements made adjacent to the casing show the track of the developing tip leakage vortex as a strip of high turbulence levels that grows across the passage.

Similar observations of mean secondary flow patterns showing tip-leakage vortices exiting rotor-blade rows have been made by Stauter,[19] Goto,[20] Puddu,[21] and Foley and Ivey.[22] Stauter's measurements, on the second-stage rotor of a two-stage machine with a tip gap of 1% chord, show the circulating flow of the tip-leakage vortex first at the 42% chord location. Although this vortex appears to wax and wane (it could not be discerned at 63 and 93% axial chord), it appears as the dominant component of the secondary flow structure at the last measurement station, 30% chord downstream of the trailing edge. In Stauter's flow the tip-leakage vortex is associated with an axial velocity defect at all stations. Foley and Ivey[22] studied an isolated rotor with a nonuniform inflow, a thin casing boundary layer (no more than a few percent chord), and a 1.65%-chord tip gap. Their measurements, which include turbulence levels measured with a laser transit anemometer, show the path of the vortex inside the blade passage. This originates from the suction side at about 30% chord and crosses the passage to the pressure side near the trailing edge. They observe that the turbulence levels reach maxima in the vortex at 35% and 80% axial chord. The same technique was used by Ivey and Swoboda[23] in the rotor passage of a four-stage machine. Their measurements at 66, 96, and 122% axial chord show a growing region of high (11%) turbulence levels associated with the leakage vortex.

Goto[20] examined the flow through a single-stage compressor rotor with a thick inlet boundary layer (about 40% chord) and varying tip gap (0.7 to 3% chord). His measurements show the rotor-tip vortex clearly visible in dynamic head contours and secondary flow vectors at the 122% axial chord station. These hot-wire results include profiles of total unsteadiness and velocity spectra at the rotor exit measured from a fixed frame of reference. The spectra show a general rise in high-frequency spectral levels in the vicinity of the casing, suggesting the presence of small-scale turbulence in the region containing the tip-leakage vortex.

Puddu[21] used phase-locked hot-wire anemometry to measure the flow up to 40% axial chord downstream of an isolated fan rotor with a thick inlet boundary layer (about 50% tip chord) and a nonuniform inflow generated by the blunt nose of the hub. The low solidity (0.42) and flow coefficient of this configuration distinguished it from the other compressor rotors already discussed and indeed the type of aircraft engine fan of relevance to this study. However, Puddu's results are unique in that they include cross sections of all mean flow velocities and Reynolds stresses. These measurements, consistent with those of other workers, show the tip-leakage vortex to be a region of intense turbulent activity. However, most of these fluctuations are seen in components parallel to the casing. In contrast to the flow studied by Lakshminaraya et al.,[4] the radial velocity fluctuations and the Reynolds shear stresses associated with them are the least important components of the turbulent fluctuations in the tip-leakage vortex.

Of the relevant studies of axial pump flows, the first was probably from Rains,[24] who used cavitation to visualize tip-leakage flows. Rains' photographs clearly show the vortex core forming toward the leading edge of the blade and trailing downstream across the passage for a range of tip gaps (0.2 to 5.2% chord) and flow rates. More detailed observations of a pump rotor flow are provided through in the studies published by Zierke et al.,[25] Straka and Farrell,[26] Farrell and Billet,[27] Zierke et al.,[28] and Zierke and Straka[29] on the Penn State HIREP (High Reynolds Number Pump). This rig consists of a rotor downstream of a set of inlet guide vanes. Two different rotor configurations of different solidity (0.43 and 0.56) were studied for a range of tip gaps 0.9–5.9% tip chord). The visualizations of Zierke et al.[25] show the tip-leakage vortex rolling up on the suction side of the tip gap near the leading edge (typically 15% chord) and remaining close to the suction surface until the 80% chord location, at which point it migrates away from the blade across the passage. The same visualizations show the shedding of a second corotating vortex from the trailing-edge tip that crosses the flow to merge with the tip-leakage vortex a short distance downstream of the trailing edge. Based on surface flow visualizations, Zierke et al. infer that this second vortex is shed as a result of centrifugal effects and the separation of the flow on the suction side of the blade just upstream of the trailing edge. Zierke et al. observe that the tip-leakage vortex is a highly unsteady structure, subject to wandering and kinking motions in the passage and downstream. Similar unsteadiness is discussed in the work of Goto.[20]

One would expect the physical structure, if not quantitative features, of the flow through the tip region of an axial compressor or pump rotor to be well reproduced by a linear cascade models, especially at lower blade loadings when centrifugal effects are less likely to be important. Cascade models are desirable in that they tend to produce large-scale flows fixed with respect to the rotor-blade frame that are more easily measured. Building a realistic cascade model is not easy, however, because the relative motion between the blade tips and casing can be an important boundary condition affecting the leakage flow and its evolution. Several investigators have performed studies of linear cascades of compressor blades with stationary endwalls. Kang and Hirsch[30–32] studied the flow through a fairly heavily loaded seven-bladed cascade with a thick (20% chord) inlet boundary layer, for a range of tip gaps (from 0 to 3.3% chord) and two inflow angles. Their detailed mean-flow measurements, at 2% tip gap, show a round tip-leakage vortex forming near the suction side of the blade leading edge. The vortex grows approximately linearly with downstream distance, but, rather than crossing the passage, it remains attached to the suction side of the blade tip, a result attributed to the lack of relative motion between blade tip and endwall. In a discussion of this work, Cumpsty and Greitzer (see Ref. 31) suggest that the fine detail of the endwall region measurements in these studies might well be different than that seen in compressor rotor flows, not so much because of the absence of relative wall motion, but because of the absence of skew that it produces in the inlet boundary layer, when seen from the rotor blade frame of reference.

Storer and coworkers[33–35] studied the development of the leakage flow under the central blade of a five-bladed linear cascade with a thin (approximately 1% chord) inlet turbulent boundary layer for tip gaps between 0.5 and 4% of the blade chord. Although cross-sectional mean-velocity measurements made at the cascade exit for 1 and 2% tip gap show a similar structure to that observed by Kang and Hirsch, they focus most of their attention on flattened pitot and hot-wire measurements of the tip-gap flow itself. They observed that the flow out of the tip gap consists of a more or less inviscid vena contracta bounded by a thin, intense shear layer formed by the separation of the flow from the pressure-side corner of the blade tip.

Altogether, the preceding studies have revealed much about tip-leakage flows and the mean flow structures and losses they produce in blade passages and immediately downstream. It has been demonstrated, at least in the vicinity of the blade row, that tip-leakage vortices are regions of concentrated turbulent activity. However, beyond this, the turbulence structure of the blade tip wake is not well understood. There have been no measurements of turbulence in tip-leakage flows extending more than a fraction of a chord length downstream of the blade row and no measurements of sufficient detail to reveal the internal turbulence structure of the tip-leakage vortex, its balance of turbulence kinetic energy, and the dominant turbulence-producing mechanisms and coherent structures. This type of information is needed if we are to be able to predict the necessary properties of these flows as they impinge on downstream stators or other devices, particularly when the stator-rotor separation distance is large.

The purpose of this study has been to provide this information. We have chosen to focus on the flow downstream of a linear cascade producing a large-scale, easily studied, tip-leakage flow. We have simulated and examined the effects of the important relative motion

between blade tip and casing, by using a moving endwall extending both upstream and downstream of the blade row. We have made detailed single- and two-point three-component turbulence measurements in these flows over a range of positions extending from the trailing edge to almost three axial chordlengths downstream, for a range of tip gaps.

In Part 1 of this series of papers we present the baseline study[36] of the mean flow and turbulence structure of the tip-leakage flow with stationary endwall. In Part 2[37] we examine the effects on this structure of relative motion between the blade tips and endwall. In Part 3[38] we observe the space–time correlation structure of the tip-leakage vortex through two-point measurements.

Apparatus and Instrumentation

Wind Tunnel

Measurements were made in the Virginia Tech Low Speed Cascade Wind Tunnel. The test section of this facility, described in detail by Muthanna,[36] houses a linear compressor cascade with adjustable tip gap. The facility is powered by a 15-hp centrifugal blower that supplies air to a settling chamber terminated by a 6.43:1 contraction. Flow from the contraction enters the upstream part of the test section, a rectangular duct with a cross section 305 mm high by 762 mm wide. At test speed the potential core of the flow through this duct is uniform to within 1% and has a streamwise turbulence intensity of 0.2% (Ref. 39).

The eight-bladed cascade is mounted diagonally across this duct, the leading-edge plane making an angle of 24.9 deg to the duct axis (Fig. 1). Two 25-mm-high boundary-layer scoops located on the upper and lower endwalls remove the duct boundary layers 241 mm upstream of the blade leading-edge plane (Figs. 1 and 2). These also reduce the section height to 254 mm. The amount of flow removed by the scoops depends on the pressure difference between flow inside the test section and the ambient, controlled by backpressure screens placed across the wind-tunnel exhaust. Removing more than the 25-mm slice of the duct flow adjacent to the endwall causes the potential core to experience a deceleration as it passes between the scoops. Indeed, about a 4% deceleration was present in the experiments reported here, raising concern that there might be some associated turning of the flow. However, measurements made in the potential core downstream of the scoops showed the flow to be aligned with the tunnel axis to within the measurement uncertainty of about 0.7 deg.

New pitchwise-uniform endwall boundary layers grow from the leading edges of the scoops. The lower endwall boundary layer (which ultimately encounters the blade tip gap) is tripped using a 9.6-mm-wide strip of 0.5-mm-diam glass sanding beads spread in a single layer beginning 135 mm upstream from the leading-edge plane. Single hot-wire measurements of the new boundary layer on the lower endwall made in the blade-passage center at the leading-edge plane showed its properties at this location to be essentially

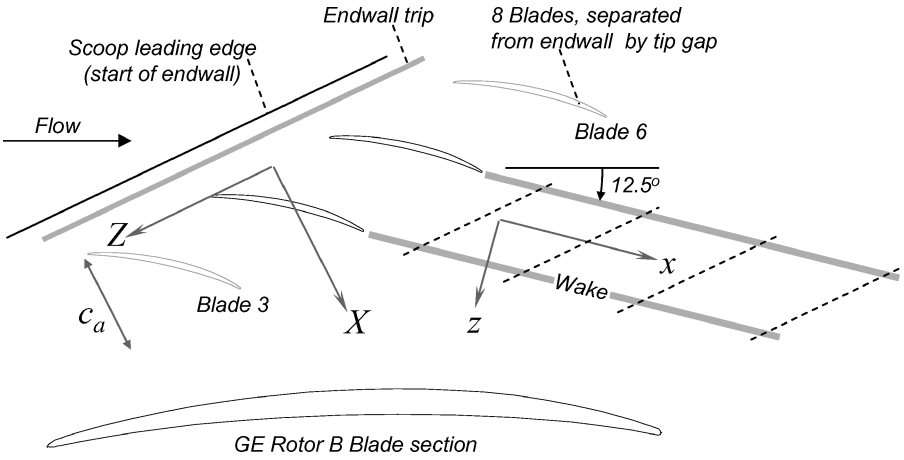

Fig. 1 Plan of cascade, with enlarged view of blade section: - - - -, locations of cross-sectional three-component turbulence measurements.

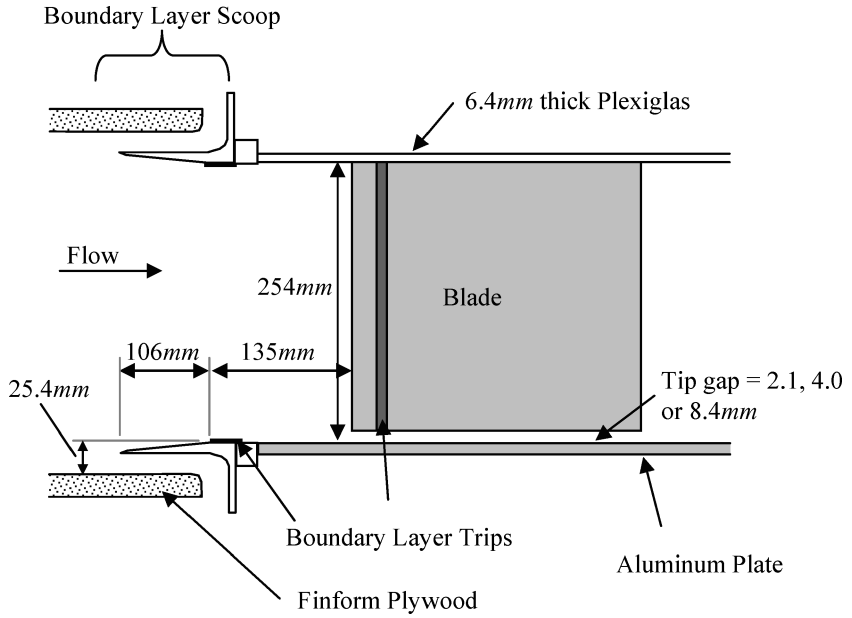

Fig. 2 Cross section through the cascade taken along the inlet flow direction.

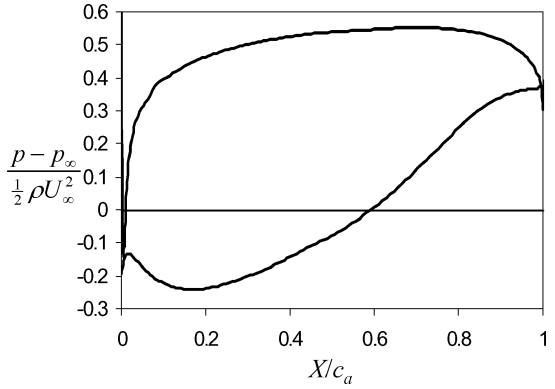

Fig. 3 Surface-pressure distribution on the blade section, from the two-dimensional cascade calculation of Shin et al.[43]

identical for the three center passages of the cascade. These properties are boundary-layer thickness 5.6 mm, displacement and momentum thickness 0.77 and 0.55 mm, and momentum thickness Reynolds number 860.

Flow downstream of the cascade is guided by the upper and lower endwalls, which remain parallel and separated by 254 mm, and two tailboards forming the sidewalls. The tailboards are hinged to the trailing edges of the two outside blades of the cascade (blades 1 and 8). The angle of the tailboards was chosen to minimize the pitchwise pressure gradient across the cascade, this being sensed using taps cut into an aluminum plate embedded in the endwall underneath the cascade. Following the pressure measurements, the entire cross section of the flow 254 mm axially downstream of the cascade was surveyed using single hot-wire anemometry, revealing a closely periodic flow in the three passages between blades 3 and 6.

The cascade itself consists of eight 254-mm-chord blades cantilevered from an aluminum superstructure and inserted into the flow through shaped slots in the upper endwall of the test section. The blades spanned the entire section height of 254 mm less the tip gap, nominally 2.1, 4.0, or 8.4 mm. Chordwise variations in the tip gaps (caused by unevenness in the endwall) were about ± 0.4 mm, with the leading edge generally slightly closer to the endwall than the trailing edge. The blades were mounted with a stagger angle 56.9 deg, a solidity of 1.076, and an inlet angle of 65.1 deg. These settings and the blade shape (a 4%-thick modified circular-arc section) match those of the tip region of the General Electric core-compressor rotor B, designed and studied by Wisler.[40,41] We chose this configuration because computational-fluid-dynamics studies[42–44] showed it to produce a blade loading (Fig. 3) qualitatively similar to that seen in a subsonic aircraft engine fan at takeoff conditions. Coincidentally, this loading distribution is also similar to that seen in some propulsion pump rotors.[25] The blades were fabricated from aluminum using a numerically controlled milling machine and supplied section data. The blunt blade tips were individually machined to sharp clean edges. Boundary-layer trips (consisting of 6-mm-wide strips of 0.5-mm-diam glass beads) were applied to both surfaces of each blade 25.4 mm downstream of the leading edge. Measurements reported by Muthanna[39] showed the flow downstream of the cascade to be independent of the form and extent of the trip. Following the adjustment of the tailboards, the cascade was found to produce 12.5 deg of turning—compared to a design value for the compressor of 12.9 deg.

For all of the present measurements, the lower endwall beneath the cascade blade tips consisted of a fixed horizontal surface. Oil-flow visualizations were performed on this surface using a mixture of kerosene, titanium dioxide, and oleic acid. The wind tunnel also has a moving belt facility that allows relative motion between this endwall and the blade tips. This is described in Part 2 of this study.

Hot-Wire Anemometry

Velocity measurements were made downstream of the cascade using the hot-wire system described by Wittmer et al.[45] Miniature four-sensor probes (Auspex Corp. Type AVOP-4-100) were used. These probes consist of two orthogonal X arrays with each sensor inclined at a nominal 45 deg to the probe axis. The total measurement volume is approximately 0.5 mm^3. The probe stem (roughly aligned with the flow) placed the measurement volume about 150 mm upstream of the 9.3-mm-diam vertical rod used for support. The rod was held by a computer-controlled traverse gear located outside of the test section and passed through a 12.7-mm-wide slot in the upper endwall of the tunnel. Scotch tape was used to minimize the amount of air leaking through the slot. The uncertainty in traverse positions was 0.1 mm.

Each sensor was operated using a Dantec 56C17/56C01 constant temperature anemometer unit. The anemometer bridges were optimized to give a matched frequency response greater than 25 kHz. Magnitude and phase response calibrations were measured for each sensor/cable/bridge combination by illuminating the probe with the beam of a pulsed YAG laser with the probe in the flow. The laser pulses are sufficiently short to appear as impulses to the hot-wire system, and thus the bridge outputs reveal the full dynamic response.

For velocity measurements the output voltages from the anemometer bridges were recorded using a PC with an Analogic 12 bit HSDAS-12 A/D converter. Hot-wire signals were buffered by four $\times 10$ buck-and-gain amplifiers containing resistance–capacitance filters to limit their frequency response to 50 kHz. The A/D converter also sampled voltage outputs from an Omega model DP80 digital thermometer and Setra model 239 pressure transducer. These devices, connected to an Omega copper-constantan thermocouple and 3.1-mm-diam Dwyer pitot-static probe, were used to continuously monitor the flow temperature and dynamic pressure in the potential core of the duct flow upstream of the cascade and thus the inlet conditions to the cascade.

Probes were calibrated for velocity before and after each sequence of measurements by placing them in the uniform jet of a TSI calibrator and using King's law to correlate the wire output voltages with cooling velocities. Velocity components were determined from the cooling velocities by means of a direct angle calibration, described in detail by Wittmer et al.[45] To generate this calibration, the probe was pitched and yawed over all likely flow angles in the calibrator jet. Comparing the known pitch and yaw angles with the probe outputs gives the true relationship between the cooling velocities and the flow angle. Hot-wire signals were corrected for ambient temperature drift using the method of Bearman.[46]

Results and Discussion

Results are presented using two coordinate systems. The blade-row aligned system (X, y, Z), defined in Fig. 1, is used to indicate positions from an origin on the lower endwall at the center of the leading-edge plane of the cascade. The system (x, y, z), aligned with the potential core flow downstream of the cascade, is used as the basis for defining flow variables for the wake region, particularly the mean and fluctuating velocity components (U, V, W) and (u, v, w). The y coordinate, representing distance from the lower endwall, is the same in both systems. Coordinate directions in the two systems are related by a 52.6-deg rotation about the y axis (inlet angle of 65.1 deg less turning angle of 12.5 deg). Most distances are normalized on the total blade chord c of 254 mm or its axial (X-wise) component c_a of 139 mm. Most velocities are normalized on the inlet velocity in the potential core upstream of the cascade U_∞, which for all of the tests was set to 25.2 ± 0.3 m/s, corresponding to a chord Reynolds number $U_\infty\, c/\nu$ of $3.88 \times 10^5 \pm 2 \times 10^3$. Most measurements were made for a tip gap $t/c = 1.6\%$, equivalent to 40% of the maximum blade thickness and 70% of the inlet boundary-layer thickness. This case will be referred to as the baseline flow. Measurements were also made for $t/c = 0.8$ and 3.3%.

The flow structure downstream of the cascade was documented by making four-sensor hot-wire measurements over grids of points in four cross-sectional (Y, Z) planes at $X/c_a = 1.37$, 2.06, 2.83, and 3.77 (see Fig. 1) in the wake of the central passage of the cascade formed by blades 4 and 5. Measurements were made at all of these stations for the baseline flow. Measurements were only made at $X/c_a = 2.83$ for the smaller and larger tip gaps. Statistical

Table 1 Uncertainty estimates at 20:1 odds estimated using the method of Kline and McClintock[47]

Quantity	Uncertainty
U, V, W	$0.01U_\infty$
u^2	$0.0003U_\infty^2$
k	$0.0005U_\infty^2$
Ω_x	$0.2U_\infty/c_a$

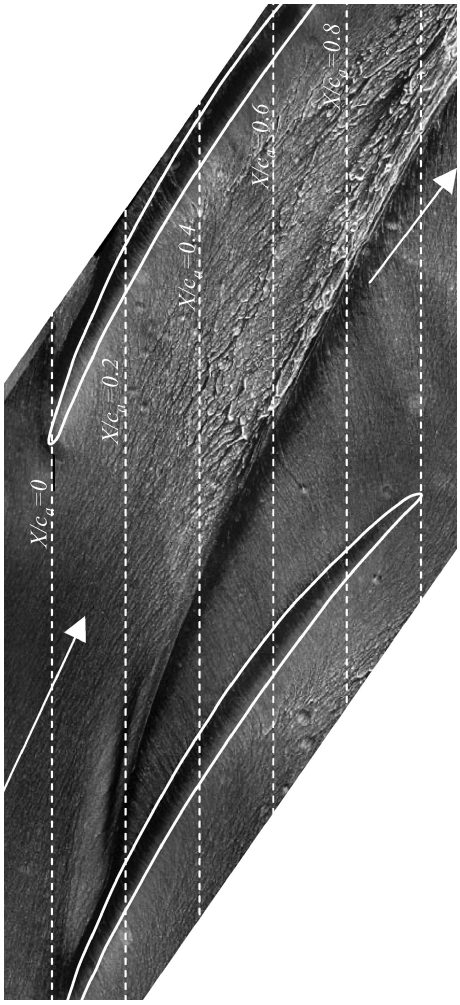

Fig. 4 Surface oil-flow visualization on the endwall for $t/c = 1.6\%$: →, inlet and outlet angles in the potential core.

flow properties (mean velocities, Reynolds stresses, triple products) were determined at each point from 30 records of 1000 samples taken at a rate of 2 kHz over a total measurement time of about 1 min. Uncertainties in measurements are listed in Table 1.[47]

Endwall Flow Visualization

Figure 4 shows an oil-flow visualization performed on the lower endwall, beneath the blade tips, for the baseline flow. Inlet and outlet angles of the potential core are shown by the arrows. White outlines are used to indicate the projection of the blade tips on to the wall. The flow through the tip gap is clearly seen in the oil streaks here. Over the forward part of the blade where the pressure difference between the pressure and suction sides is greatest (Fig. 3), the tip gap flow is directed almost perpendicular to the blade camber line. Toward the trailing edge where the loading is less, this flow is directed more toward the pitchwise direction. The dark region immediately beneath the blade is evidence of the high surface shear stress here, which has scoured away most of the oil-flow pigment. The visualization suggests that over the first 20% chord flow passing through the tip gap remains channeled in a slim region adjacent to the suction side of the blade. At about 20% chord, however, a very distinct local separation line springs from this region moving out to midpassage by the 80% chord station and then continuing toward the pressure side of the passage as the flow passes through the trailing-edge plane. Downstream of this plane (note that the actual visualization extended much further downstream than Fig. 4), this line becomes straight, making an angle of close to 5 deg with the outlet angle measured in the potential core. At least downstream of the cascade, the separation line is associated with the tip-leakage vortex (see the following). Near the 20%-chord location there is an elongated region of scouring just upstream of the separation line. Although the oil streaks marking this region are strongly distorted, there is no additional separation line, and so this cannot be a secondary vortex in contact with the wall. Whatever structure produces this feature disappears from the visualization downstream of the 20%-chord station, suggesting it either rapidly dissipates or is lifted away from the endwall.

This picture appears consistent with near-endwall flow patterns observed by previous researchers studying cascade rotor-tip flows with comparable characteristics. In particular the shape of the separation line and the direction of the flow in the tip gap bear a close resemblance to the vortex trajectories and leakage flow directions seen by Inoue and Kuroumaru.[18] Lakshminarayana and coworkers[3,5,10,13] also report the leakage flow originating near the 25%-chord location, and crossing the passage on a trajectory similar to that seen here. Ironically, the present results bear much less resemblance to the linear cascade endwall visualizations of Kang and Hirsch.[30] For a tip gap of 2% chord, they also observe the shedding of a separation line from the tip gap region, but the line and associated tip-leakage vortex remain close to the suction surface of the blade. Comparison with the present experiment shows that this behavior cannot explained solely by the absence of relative motion between the blade tip and endwall, as postulated by Kang and Hirsch.[31] Instead, this behavior might have more to do with the relatively small inlet angle of Kang and Hirsch's configuration (29.3 deg), the high loading and the shape of their blades, which concentrated most of the camber towards the trailing edge.

Flowfield Just Downstream of the Cascade

Figure 5 shows the structure of the baseline flow at $X/c_a = 1.37$ in terms of mean crossflow velocity vectors (V, W), and contours of mean streamwise velocity U/U_∞ and vorticity $\Omega_x = \partial W/\partial y - \partial V/\partial z$ normalized on U_∞/c_a. Vorticity was calculated by numerical differentiation of the mean-velocity data, assuming streamwise derivatives (in x) to be negligible. The vectors are drawn at the actual measurement points and thus also show the L-shaped measurement grid. The aspect ratio of the plots has been adjusted (by shrinking the Z axis) so as to reveal the flow as it would appear if viewed from downstream along the x axis. That is, equal distances on the vertical and horizontal axes represent equal distances in y and z. Pitchwise locations are shown relative to the center of the wake of blade 4 (at $Z = Z_w$) to simplify the comparison with downstream locations to be made later. The separation line location observed in the endwall flow visualizations is marked on the plots.

The mean velocity and vorticity fields (Fig. 5) are dominated by three features: the potential core, the vertical wakes of blades 4 and 5, and, adjacent to the end wall, the tip leakage vortex. Away from the endwall the wakes [centered at $(Z - Z_w)/c_a = 0$ and -1.7] are approximately straight and two dimensional, and the potential core between them is almost uniform. The mean velocity in the core is $0.74U_\infty$. The wakes have centerline streamwise velocity deficits of between 0.24 to $0.28U_\infty$ and half-widths (measured from the centerline to the point where the deficit is half its centerline value) of close to $0.1c_a$. Perhaps surprisingly the wakes have an impression both on the mean vorticity and secondary flowfields. The wake of blade 4 [at $(Z - Z_w)/c_a = 0$] includes a vertical strip of positive vorticity near its center flanked by two negative strips to either side (Fig. 5c). These regions are associated with spanwise flows in opposite directions along the two sides of the wake (Fig. 5a). These spanwise flows are not strong (constituting a deflection of the flow by only about 1 or 2 deg from the potential core direction)

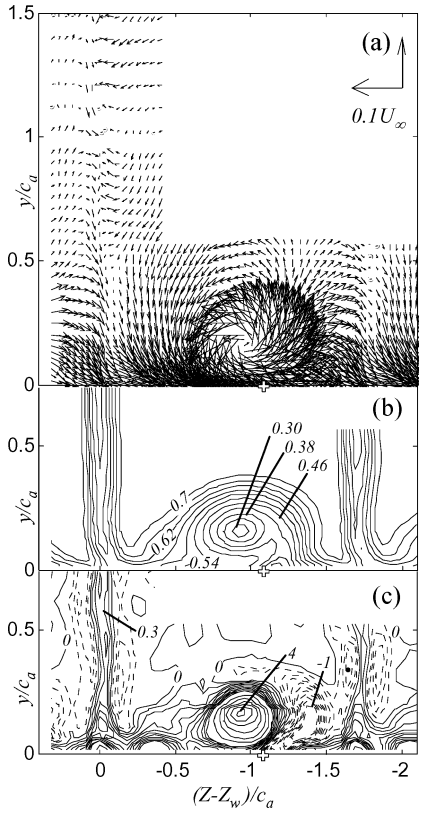

Fig. 5 Mean flow quantities at $X/c_a = 1.37$ for the 1.6% chord tip gap: a) vectors of mean crossflow velocity (V, W); b) contours of U/U_∞ in steps of 0.04; and c) contours of mean streamwise vorticity $\Omega_x c_a/U_\infty$ in intervals of 0.1 from −1 to 1 and intervals of 0.5 from 1.5 to 4. Negative levels are shown dashed. Symbol on Z axes indicates separation line location.

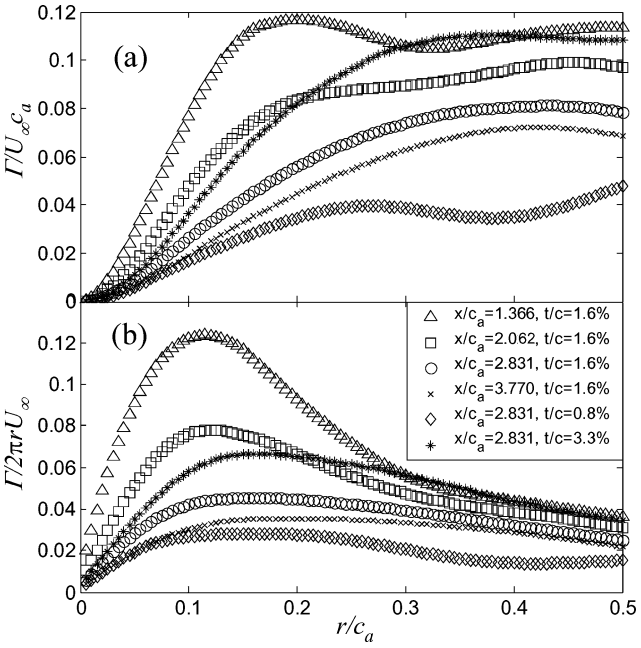

Fig. 6 In the tip-leakage vortex as a function of radius r from its center: a) circulation profiles and b) corresponding circumferentially averaged tangential velocity profiles.

and do not appear to be associated with significant shedding of lift from the blades away from the endwall. Presumably they are remnants of slight three dimensionality in the blade boundary layers.

The endwall region between the wakes is dominated by the tip-leakage vortex shed by blade 4. By this station the vortex has crossed the passage to a point about 60% of the way from the wake of blade 4 to that of blade 5. The vortex produces almost circular contours of positive vorticity (Fig. 5c) centered around $y/c_a = 0.17$, $(Z - Z_w)/c_a = -0.93$, where Ω_x reaches its peak value close to $4U_\infty/c_a$. We will use the peak vorticity location as the definition of the vortex center. The vortex also produces a clearly defined rotating flowfield that extends about $0.35c_a$ from the endwall and over a pitchwise distance of about $0.8c_a$. The maximum measured secondary flow velocity of $0.21U_\infty$ occurs at $y/c_a = 0.02$, $z/c_a = -0.87$, a point more or less directly beneath the vortex center.

The vortex also produces an oval region of streamwise mean velocity deficit. In general, the velocity differences associated with the deficit are considerably larger than those associated with the crossflow. The maximum deficit, occurring at the vortex center is $0.44U_\infty$, more than twice the peak crossflow velocity and substantially larger than the maximum deficit appearing in the two-dimensional portions of the blade wakes. Mayer and Powell[48] show theoretically that this situation is unstable when it occurs in a free vortex. Ragab[49] shows, using direct numerical simulation, that this instability results in the formation of helical turbulent structures that encircle the core. One might therefore reasonably expect such structures in this case.

Figure 5 shows the z location of the separation line observed on the oil-flow visualizations at this station. Although it is difficult to see in Fig. 5a, the mean secondary flow is moving slowly away from the endwall in this region. This action presumably lifts low-momentum fluid away from the endwall, which would explain the small region of streamwise mean-velocity deficit that surrounds the separation line in Fig. 5b. This near-wall fluid would also carry negative streamwise vorticity produced by the shear between the crossflow velocity field of the vortex and the no-slip condition at the endwall. Thus, not surprisingly, Fig. 5c shows a tongue of negative vorticity emanating from the vicinity of the separation line. However, the size of this region (which winds about halfway around the vortex) and its intensity suggest that it might have a second cause. One candidate is the secondary structure visible suggested in the oil flow visualizations near the blade leading edge.

Regardless of its origin, the negative vorticity wrapped around the vortex might indicate a second type of instability in the mean flowfield. This can be seen in the circulation distribution $\Gamma/U_\infty c_a$ of the leakage vortex, plotted as a function of radius r/c_a from the vortex center in Fig. 6. Circulation was computed by integrating the mean streamwise vorticity of Fig. 5c over circles (as seen from along the x axis) concentric with the vortex center. Contributions from areas outside the measurement grid (portions of the freestream, the bottom of the endwall boundary layer) were ignored. The tip-leakage vortex at $X/c_a = 1.37$ has a well-defined circulation distribution, but the circulation does not increase monotonically from the vortex center. Instead, as a result of the tongue of negative vorticity, it reaches a maximum of 0.117 at a radius of $0.20c_a$ and then falls by about 10%. This is 21% of the total bound circulation implied by Fig. 3. According to Rayleigh's criterion, this would be centrifugally unstable in an axisymmetric vortex. Wittmer and Devenport[50] studied the behavior of a wing-tip vortex destabilized by a neighboring region of negative vorticity somewhat similar to that seen here. They found intense turbulence production between the two opposing regions as a result of cross-stream turbulence stresses and velocity gradients (i.e., those associated with V, W, v, and w).

Overall, the structure of the mean flowfield at this station bears quite a close resemblance to that seen in the in the compressor rotor flow of Inoue and Kuroumaru.[18] Their rotor with an inlet angle of 60 deg and tip gap of 1.7%-chord, shows similarly positioned tip-leakage vortex and blade wakes. Even the shape of the region of axial velocity deficit associated with the vortex is similar, the ratio of the pitchwise width to height of the vortex being about three, as in the present flow (Fig. 5b).

The turbulence structure of the flow at this station is illustrated in Fig. 7 in terms of contours of turbulence normal stress $\overline{u^2}/U_\infty^2$, turbulence kinetic energy $k/U_\infty^2 = \frac{1}{2}(\overline{u^2} + \overline{v^2} + \overline{w^2})/U_\infty^2$, and turbulence kinetic energy production and diffusion normalized on U_∞

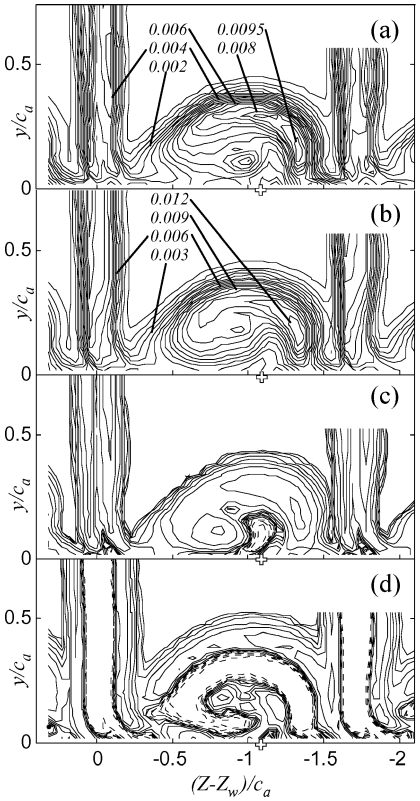

Fig. 7 Contours of turbulence quantities at $X/c_a = 1.37$ for the 1.6%-chord tip gap: a) u^2/U_∞^2 contours in steps of 0.0005; b) k/U_∞^2 contours in steps of 0.00075; and c) production and d) diffusion of k normalized on c_a and U_∞, where contour levels are ±0.0001, ±0.00017, ±0.0003, ±0.0006, ±0.001, ±0.0017, 0.003, 0.006, 0.01, and 0.017. Negative levels shown dashed.

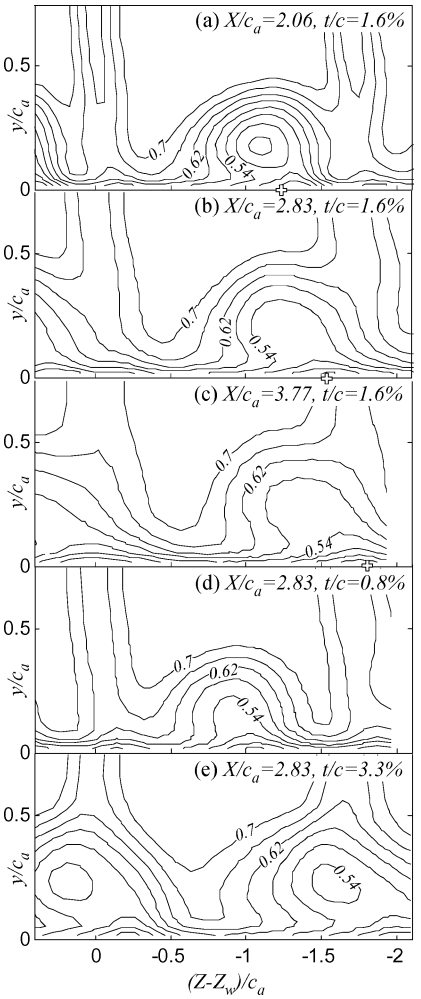

Fig. 8 Contours of U/U_∞ as functions of streamwise position and tip gap. Contours in steps of 0.04. Symbols indicate separation line locations.

and c_a. Production and diffusion were estimated from the measured mean velocities, Reynolds stresses, and triple products by numerical differentiation and by ignoring derivatives in the streamwise x direction. Figures 7a and 7b show high turbulence levels both in the blade wakes and the region containing the leakage vortex. Interestingly, in the near two-dimensional region away from the endwall the wakes have the same double-peaked $\overline{u^2}$ profile and a single-peaked k profile one would expect to see in a fully developed plane wake (e.g., Refs. 51 and 52). Peak values of $\overline{u^2}$ and k in the almost two-dimensional regions defining the blade wakes are around $0.0065U_\infty^2$ and $0.0105U_\infty^2$, respectively. Turbulence levels are somewhat larger in the tip-leakage vortex. Both $\overline{u^2}$ and k reach their maximum values of $0.009\ U_\infty^2$ and $0.012U_\infty^2$, respectively, to the right of the vortex center in an arc that borders the top and right-hand sides of the vortex core. This region coincides closely both with the tongue of negative streamwise vorticity (Fig. 5c) and the area of strongest U gradients associated with the streamwise velocity deficit of the vortex (Fig. 5b). Contours of $\overline{v^2} + \overline{w^2}$ (not shown) show similar distribution turbulence levels, although individually these stresses show some differences associated with the resolution of the roughly circular turbulence field of the vortex into Cartesian components. This is not to say, however, that the turbulence in the vortex is isotropic. Consistent with Puddu's[21] measurements in a fan wake (and at odds with Lakshminarayana et al.[4]), we find that turbulent fluctuations components parallel to the endwall are dominant $\overline{u^2}$ and $\overline{w^2}$ being on average about 20% larger than $\overline{v^2}$. In addition the $\overline{uv}$ and $\overline{uw}$ shear stresses are substantially greater than $\overline{vw}$ in the endwall region.

Figure 7c shows the turbulence production to be primarily centered on the regions of high turbulence levels, particularly the two sides of the blade wakes, and the arc surrounding the vortex. The arc is more complete in the production distribution, extending down the left-hand side and a short distance beneath the vortex center. The diffusion (Fig. 7d) is negative in these regions of high production and positive in the surroundings, showing clearly the action of this term in redistributing the high turbulence levels. The mechanism responsible for the turbulence generation can, to some extent, be inferred from by examining the component contributions to the production. Without x derivatives the production can be written as

$$-\overline{uv}\frac{\partial U}{\partial y} - \overline{uw}\frac{\partial U}{\partial z} - \overline{v^2}\frac{\partial V}{\partial y} - \overline{w^2}\frac{\partial W}{\partial z} - \overline{vw}\left(\frac{\partial V}{\partial z} + \frac{\partial W}{\partial y}\right)$$

The first two terms, which represent production by streamwise velocity gradients, are dominant, both in the blade wake regions and in the arc-shaped region surrounding the vortex. It therefore seems likely that instability associated with the streamwise velocity deficit is primarily responsible for the turbulence structure. The remaining cross-stream terms remain small, except in the part of the arc to the lower left of the vortex center. Integrating the production terms over the cross-sectional area of the endwall flow shown in Fig. 7 (i.e., from the wall to $y/c_a = 0.7$ and over one period in Z), we find that in total U-gradient terms contribute close to 84% of the total production of turbulence kinetic energy.

Development of the Flow with Distance Downstream

The streamwise development of the baseline flow is shown in Figs. 8–11 in terms of cross sections of streamwise mean velocity U/U_∞, vorticity $\Omega_x c_a/U_\infty$, turbulence kinetic energy k, and turbulence kinetic energy production measured at $X/c_a = 2.06$, 2.83, and 3.77. The variation of the mean-velocity field with X provides some checks on the measurements. Figure 12 shows the trajectory

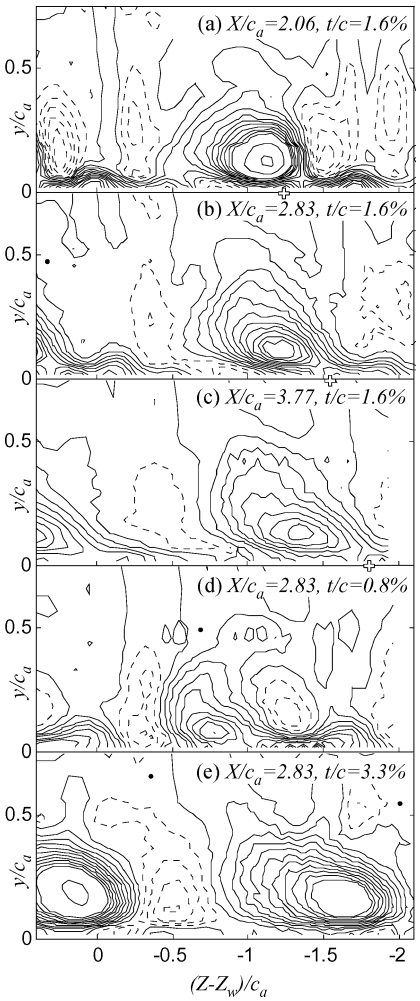

Fig. 9 Contours of mean streamwise vorticity $\Omega_x c_a/U_\infty$ as functions of streamwise position and tip gap. Contours are in intervals of 0.1 from −1 to 1 and intervals of 0.5 from 1.5 to 4. Negative levels are shown dashed. Symbols indicate separation line locations.

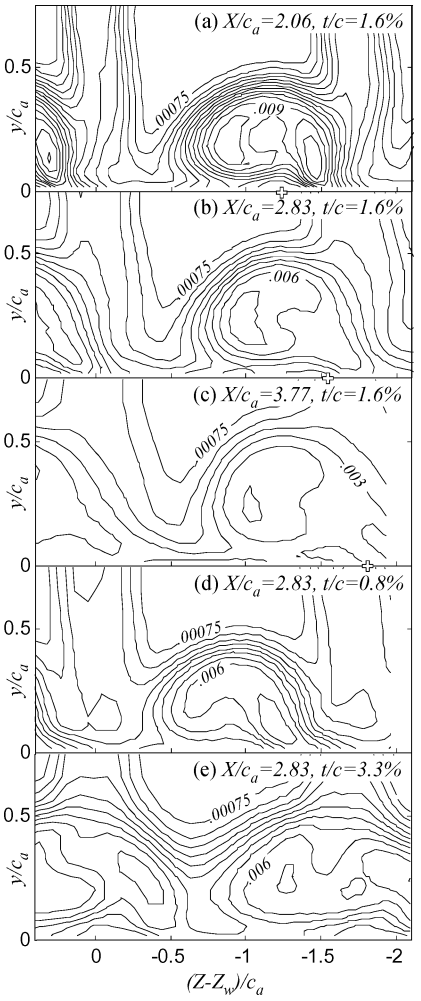

Fig. 10 Contours of turbulence kinetic energy k/U_∞^2 as functions of streamwise position and tip gap. Contours are in intervals of 0.00075 from 0.00075. Symbols indicate separation line locations.

of the center of wake of blade 4, Z_w, at the midheight of the cascade ($y/c_a = 0.916$), defined by the locus of minimum streamwise velocity. This is closely consistent with the 12.5-deg turning angle. The mean-velocity data can also be integrated to determine the total mass flux (over one period) at each cross section. Mass flux was found to vary by less than ±1% from $X/c_a = 1.37$ to 3.77.

Away from the endwall Figs. 8–11 show the growth of the blade wakes, the accompanying weakening of their streamwise velocity deficit, and the decay of their turbulence fields. This evolution, which is particularly useful as a benchmark against which to judge the growth and decay of the vortex, is summarized in Fig. 13 in terms of the streamwise variations of wake half-width L_w/c_a, peak velocity deficit U_w/U_∞, and peak turbulence kinetic energy k_w/U_∞^2 determined from measurements through the wake blade 4 at $y/c_a = 0.916$. Despite its short development length, this wake displays many of the characteristics of a fully developed flow. L_w/c_a increases with the square root of X, and U_w/U_∞ decreases approximately with its inverse, from a virtual origin near $X/c_a = 0.9$. The peak turbulence level k_w/U_∞^2 decays such that the ratio k_w/U_w^2 is almost constant at around 0.24 from $X/c_a = 2$ downstream. In addition, Muthanna[36] shows the normalized mean-velocity and turbulence stress profiles in this wake to have reached an apparently fully developed form by $X/c_a = 2$.

Figures 8 and 9 together with Figs. 5b and 5c show the parallel evolution of the vortex. In the mean flowfield, the vortex grows, weakens, and becomes distorted by its interaction with the endwall. By the last two stations the initially circular vorticity contours associated with the core have taken on a distinctly elliptical form with a major axis at about 15 deg to the endwall (Fig. 9). At the same time the streamwise mean velocity field loses its minimum at the vortex center, and, as the vortex progresses across the endwall, the regions of deficit associated with the vortex and the wake of blade 5 begin to merge.

We can quantify the position of the vortex in terms of the trajectory of its center (defined as the point of maximum Ω_x), plotted in Figs. 12 and 13. This trajectory closely follows the endwall separation line, the two diverging only slowly with X. Looking at the streamwise velocity cross sections (Fig. 8), this divergence appears simply to be caused by the growth of the vortex, rather than any independence of behavior. Indeed, the separation line remains at the center of the thin low-velocity region adjacent to the endwall where the vortex appears to be gently lifting fluid from the wall. Over the range of positions studied, the vortex center makes an angle of about 6 deg with the potential core, presumably caused by induction by its image in the endwall. It also moves closer to the endwall (Fig. 13b) from $y/c_a = 0.17$ at $X/c_a = 1.336$ to 0.13 at $X/c_a = 3.77$.

The decay of the crossflow velocity field produced by the vortex can be quantified in terms of the mean streamwise vorticity at its center, which falls from close to 4 at $X/c_a = 1.37$ to about 0.7 at $X/c_a = 3.77$. The decay is also captured in the profiles of mean circulation about the vortex center (Fig. 6). Over the measured length of the flow, the peak circulation drops from near $0.12 U_\infty c_a$ to about $0.07 U_\infty c_a$, and the rate of increase of circulation with radius also falls. Significantly, the circulation profile loses its overshoot between $X/c_a = 1.37$ and 2.06 as a result of the weakening and redistribution of the negative vorticity region (Fig. 9). This region lifts away from the endwall and does not move with the separation

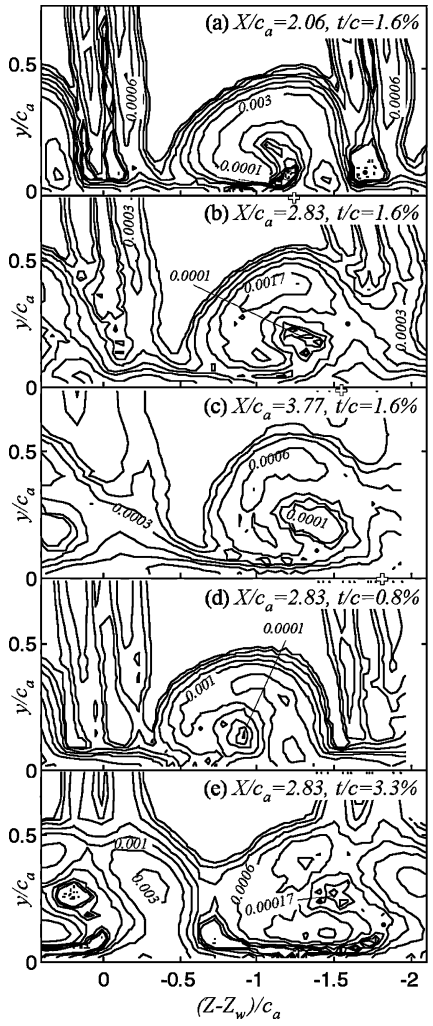

Fig. 11 Contours of turbulence-kinetic-energy production normalized on c_a and U_∞ as functions of streamwise position and tip gap. Contour levels are −0.0017, −0.001, −0.0006, −0.0003, −0.00017, −0.0001, 0.0001, 0.00017, 0.0003, 0.0006, 0.001, 0.0017, 0.003, 0.006, 0.01, and 0.017. Negative levels are shown dashed. Symbols indicate separation line locations.

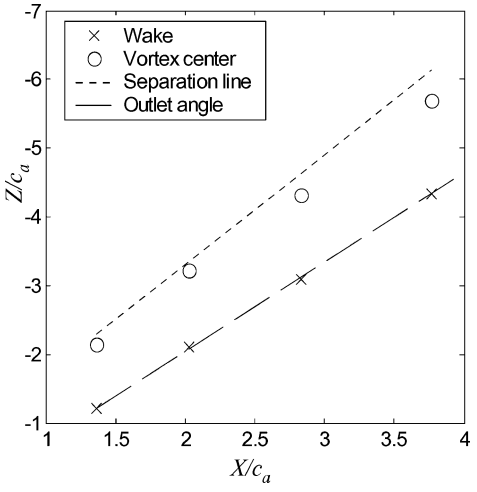

Fig. 12 Comparison of the trajectory of the vortex center, wake center, and separation line from blade 4 with the outlet angle for *t/c* = 1.6%.

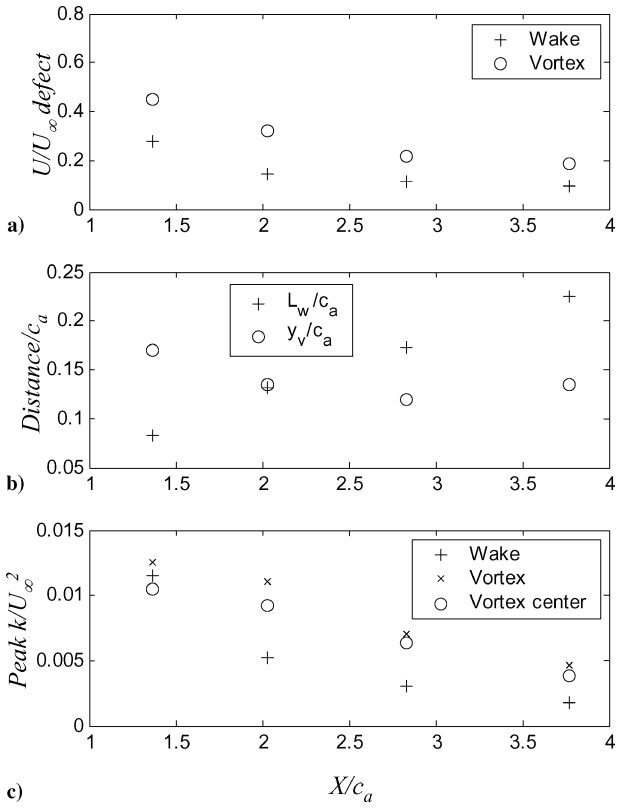

Fig. 13 Streamwise variation of a) velocity defect at the wake and vortex centers, b) wake half-width and distance of vortex center from the endwall, c) peak turbulence kinetic energy in the wake and vortex and turbulence kinetic energy at the vortex center, for *t/c* = 1.6%.

line suggesting that the alignment of these features at $X/c_a = 1.37$ might be coincidental. By $X/c_a = 3.77$ the negative vorticity has all but disappeared. Plotting circulation in terms of circumferentially averaged tangential velocity $\Gamma/2\pi r U_\infty$ (Fig. 6b) reveals a vortex core with a clearly defined peak tangential velocity and, at the two upstream locations, core radius of close to $11\% c_a$. Symptomatic of the rest of the secondary flowfield, the peak tangential velocity decays by a factor of 3.5 over the measured length of the flow.

The decay of the mean streamwise velocity field is illustrated in Fig. 13a, in terms of the deficit at the vortex center. Between the most upstream and downstream locations the deficit falls from $0.45U_\infty$ to $0.19U_\infty$, a factor of 2.4. This number, which seems representative of the rest of the streamwise velocity field in the vortex, indicates a significantly slower decay than that seen in either the secondary velocity field or in the blade wakes. The implication is that the streamwise mean-velocity deficit of the vortex, already the dominant feature of the flow at $X/c_a = 1.37$, becomes increasingly important as the flow progresses downstream.

The development of the turbulence structure of the flow with streamwise distance (Figs. 7b, 7c, 10, and 11) appears consistent with that of the mean flowfield. The turbulence kinetic energy distribution in the blade wakes broadens and weakens with X, but its essential shape remains the same (Figs. 7b and 10). In the vortex, the arc of high turbulence levels above the core broadens, rotating slowly counterclockwise about the vortex center with distance downstream. Figure 13c compares the streamwise decay of peak turbulence kinetic energy levels in the wake, the vortex, and at the vortex center. Although turbulence levels in the wake and vortex are similar at $X/c_a = 1.37$, they decay more slowly in the vortex so that by $X/c_a = 3.77$ the vortex is about twice as turbulent as the wake. The anisotropy of the turbulence seen at $X/c_a = 1.37$ persists with distance downstream with $\overline{u^2}$ and $\overline{w^2}$ remaining on average 10 to 20% larger than $\overline{v^2}$, and $\overline{uv}$ and $\overline{uw}$ remaining dominant over $\overline{vw}$ in the endwall region.

The arc of turbulent activity surrounding the vortex center remains most distinct in the turbulence kinetic energy production (Figs. 7c

and 11). This region of highest production remains quite closely consistent with the region of highest gradient in the streamwise mean velocity (Fig. 8) because production terms associated with these gradients remain dominant. Integrating those terms over the flow cross section, we find that they contribute respectively 84, 91, and 99% of the production at $X/c_a = 2.06$, 2.83, and 3.77. This seems to reinforce the conjecture that it is the instability of the streamwise velocity field (possibly producing helical turbulence structures like those seen by Ragab[49]) that produces and sustains the turbulent activity in the vortex downstream of the cascade.

Effects of Tip Gap

The effects of tip gap on the cross-sectional structure of the vortex at $X/c_a = 2.83$ can be seen by comparing the contours of mean flow and turbulence properties plotted for $t/c = 1.6\%$ in part b of Figs. 8–11 with those plotted for $t/c = 0.8$ and 3.3% in parts d and e.

Tip gap clearly has a strong effect on the position, size, and rotational strength of the vortex. The vortex center (defined by the location of peak streamwise vorticity, Fig. 9) moves across the endwall as the tip gap is increased, away from the rest of the wake shed by blade 4. The pitchwise separation between the vortex and wake centers increases from $0.77c_a$ for $t/c = 0.8\%$ to $1.22c_a$ and then $1.63c_a$ for $t/c = 1.6$ and 3.3%.

The change in the relative position of the vortex can be attributed to the change in its mean rotational strength and thus the rate at which it convects itself pitchwise across the endwall. The vorticity contours of Fig. 9 show a substantial increase in the size and intensity of the region of positive vorticity produced by the vortex as the tip gap is increased. This effect is also clearly captured in the circulation distributions of Fig. 6. The total circulation in the vortex increases from $0.04U_\infty c_a$ for $t/c = 0.8\%$ to $0.11U_\infty c_a$ for $t/c = 3.3\%$. Interestingly, the increase in circulation with radius for $t/c = 0.8\%$ is nonmonotonic, suggesting that, because of its slower rotational motion, the vortex might be in an earlier stage of its development than at the other tip gaps.

The contours of streamwise mean velocity (Fig. 8) also show the change in size and position of the vortex. However, the magnitude of the streamwise mean-velocity deficits inside the vortex appears almost unaffected by tip gap. In effect then, increase in tip gap increases the relative strength of the tangential velocity field of the vortex, when compared to its streamwise velocity field.

Turbulence kinetic energy levels in the tip-leakage vortex (Fig. 10) also remain surprisingly unaffected by tip gap. The size of the turbulent imprint of the vortex and its position on the endwall change in a manner consistent with the mean-velocity field, but the peak turbulence kinetic energy remains almost fixed at about $0.007U_\infty^2$. The distribution of turbulent kinetic within the vortex also appears largely unchanged (with the highest turbulence levels being concentrated in a arc over the top of the vortex), with the exception of some deviations in the contours apparently associated with the intersection of the wake of blade 5 and the vortex for $t/c = 3.3\%$.

The qualitative distribution of turbulence kinetic energy production within the vortex is similarly unaffected by tip gap (Fig. 11). The magnitude and makeup of the production term do, however, show some effects of the changes in the mean-velocity field produced by the increase in tip gap. With the same streamwise mean-velocity deficit spread over a larger region (Fig. 8) the gradients of U, and the corresponding dominant production terms, weaken as the tip gap increases. As a consequence, the peak magnitude of turbulence kinetic energy production fall as the tip gap is increased, particularly between $t/c = 1.6$ and 3.3%. At the same time the proportion of the total production caused by U gradients falls, from 95% for $t/c = 0.8\%$, to 90% and then 79% for $t/c = 1.6$ and 3.3%. The increasingly important (but still small) contributions from V and W gradient production terms are centered in areas to the left and right of the vortex center at $t/c = 3.3\%$.

Conclusions

Extensive measurements have been made in the flow downstream of a linear compressor cascade with tip gap. The cascade, consisting of eight 4%-thick modified circular-arc blades, was operated at a chord Reynolds number of 3.88×10^5 with a thin inlet boundary layer and 12.5 deg of turning. The tip gap was initially set to 1.6% blade chord c. Endwall oil-flow visualizations were performed in the blade passage, and three-component velocity and turbulence measurements were made in four cross sections downstream of the trailing edge ($X/c_a = 1.37$, 2.06, 2.83, and 3.77). At one station ($X/c_a = 2.83$) measurements were also made for tip gaps of $0.8\%c$ and $3.3\%c$. Overall, these measurements reveal in new detail the structure of a tip-leakage vortex wake, the manner of its decay and mechanisms of turbulence production, its dependence on tip gap, and its relationship to the two-dimensional parts of the blade wakes.

Despite the absence of relative motion between the endwall and blade tips, the apparent trajectory of the vortex through the blade passage (inferred from the visualization) and its mean-velocity distribution downstream were found to closely resemble those seen in earlier studies of compressor rotors with comparable characteristics, particularly Inoue et al.[17] and Inoue and Kuroumaru.[18] This suggests that differences between other stationary-endwall cascade studies (e.g., Kang and Hirsch[30,31]) and rotor flows might have more to do with blade loading and geometry differences than the absence of relative motion between the blade tip and endwall.

Just downstream of the cascade (at $X/c_a = 1.37$), the endwall region is dominated by the tip-leakage vortex, which produces a well-defined rotating flow (characterized by almost circular contours of streamwise vorticity) and an oval region of streamwise mean-velocity deficit. The rotating flow defines a vortex core 11% axial chord in radius, and the vortex has a total circulation equal to about 21% of the bound circulation on each blade. This vortex, however, is dominated by its streamwise mean velocity deficit, which at maximum reaches 44% of the inlet velocity, more than twice the peak crossflow velocity and substantially larger than the maximum deficit appearing in the two-dimensional portions of the blade wakes.

Moving downstream, the vortex grows, distorts, and moves across the endwall apparently under the action of its image in the wall. The vorticity contours near the vortex center become elliptical with major axes inclined at about 15 deg to the endwall. The circulation distribution becomes monotonic as the negative vorticity region dissipates. The vortex core grows, and its tangential velocity decays, by a factor of about 3.5 over the measured length of the flow. The streamwise velocity deficit of the vortex also decays, but at a significantly slower rate. It therefore becomes increasingly important as the flow progresses downstream.

Turbulence levels in the tip-leakage vortex are initially (at $X/c_a = 1.37$) highest in an arc that borders the top and upwash sides of vortex core. This region broadens and appears to be convected slowly counterclockwise about the vortex center with distance downstream. Although turbulence levels in the wake and vortex are similar at $X/c_a = 1.37$, they decay more slowly in the vortex so that by the most downstream location the vortex is about twice as turbulent as the wake. Turbulence production is low, if not negative, at the vortex center, and largest in the arc of turbulent activity. The turbulent diffusion is negative in the regions of high production and positive in the surroundings, showing the action of this term in redistributing the turbulence.

Consistent with its dominance of the mean velocity field, the streamwise mean velocity deficit of the vortex is by far the largest source of turbulence. Turbulence production terms associated with gradients of the mean streamwise velocity account for almost 84% of the production close to the trailing edge ($X/c_a = 1.37$)—a percentage that increases with distance downstream. It is speculated that much of this turbulence can take the form of helical structures wrapped around the vortex because such structures are known to be produced in free vortices when destabilized by a large streamwise velocity defect.[49]

Tip gap has a strong effect on the position, size, and rotational strength of the vortex. A factor of four increase in tip gap increases the total vortex circulation by almost three times. The stronger vortex is larger and convects itself further across the endwall. Unexpectedly, the maximum streamwise mean-velocity deficit and the turbulence kinetic energy levels inside the vortex appear almost

unaffected by tip gap. With the same deficit spread over a larger region, the gradients of streamwise mean velocity and the corresponding turbulence production terms, although still dominant, weaken as the tip gap increases.

Acknowledgments

The authors acknowledge the support of NASA Langley Research Center, in particular Joe Posey, for their support under Grant NAG 1-1801. Some of the analysis of these data was also performed with the support of the Office of Naval Research, under Grant N00014-99-1-0294, administered by Ki-Han Kim. The assistance of Greg Dudding in building and assembling the cascade wind tunnel is gratefully acknowledged. Numerical results from the experiments described here are available from the authors' Website.[‡]

References

[1]Lakshminarayana, B., and Ravindranath, A., "Interaction of Compressor-Rotor Blade Wake with Wall Boundary Layer/Vortex in the End-Wall Boundary Layer," *Journal of Engineering for Power*, Vol. 104, No. 2, 1982, pp. 467–478.

[2]Davino, R. M., "Characteristics of the Flow in the Annulus Wall Region of an Axial-Flow Compressor Rotor Blade Passage," AIAA Paper 82-0413, Jan. 1982.

[3]Lakshminarayana, B., Pouagare, M., and Davino, R., "Three-Dimensional Flow-Field in the Tip Region of a Compressor Rotor Passage, Part 1: Mean Velocity Profiles and Annulus Wall Boundary Layer," *Journal of Engineering for Power*, Vol. 104, No. 4, 1982, pp. 771–781.

[4]Lakshminarayana, B., Pouagare, M., and Davino, R., "Three-Dimensional Flow-Field in the Tip Region of a Compressor Rotor Passage, Part 2: Turbulence Properties," *Journal of Engineering for Power*, Vol. 104, No. 4, 1982, pp. 771–781.

[5]Pandya, A., and Lakshminarayana, B., "Investigation of the Tip-Clearance Flow Inside and at the Exit of a Compressor Rotor Passage. Part 1: Mean Velocity Field," *Journal of Engineering for Power*, Vol. 105, No. 1, 1993, pp. 1–12.

[6]Pandya, A., and Lakshminarayana, B., "Investigation of the Tip-Clearance Flow Inside and at the Exit of a Compressor Rotor Passage. Part 2: Turbulence Properties," *Journal of Engineering for Power*, Vol. 105, No. 1, 1983, pp. 13–17.

[7]Lakshminarayana, B., and Pandya, A., "Tip Clearance Flow in a Compressor-Rotor Passage at Design and Off-Design Conditions," *Proceedings of the 6th International Symposium on Air-Breathing Engines*, New York, 1983, pp. 468–478.

[8]Lakshminarayana, B., and Pandya, A., "Tip Clearance Flow in a Compressor-Rotor Passage at Design and Off-Design Conditions," *Journal of Engineering for Gas Turbines and Power*, Vol. 106, No. 3, 1984, pp. 570–577.

[9]Popovski, P., and Lakshminaryana, B., "An Experimental Study of the Compressor Rotor Flow Field at Off-Design Condition Using Laser Doppler Velocimeter," *Proceedings of the 7th International Symposium on Air Breathing Engines*, AIAA, New York, 1985, pp. 321–330.

[10]Murthy, K. N. S., and Lakshminarayana, B.,"Laser Doppler Velocimeter Measurement in the Tip Region of a Compressor Rotor," *AIAA Journal*, Vol. 24, No. 5, 1986, pp. 807–814.

[11]Lakshminaryana, N., Sitaram, N., and Zhang, J., "End-Wall and Profile Losses in a Low-Speed Axial Flow Compressor Rotor," *Journal of Engineering for Gas Turbines and Power*, Vol. 108, No. 1, 1986, pp. 22–31.

[12]Lakshminaryana, B., Zhang, J., and Murthy, K. N. S., "An Experimental Study of the Effects of Tip Clearance on Flow Field and Losses in an Axial Flow Compressor Rotor," *Proceedings of the 8th International Symposium on Air Breathing Engines*, AIAA, New York, 1987, pp. 273–290.

[13]Lakshminarayana, B., and Murthy, K. N. S., "Laser Doppler Velocimeter Measurement of Annulus Wall Boundary Layer Development in a Compressor Rotor," American Society of Mechanical Engineers, Paper 87-GT-251, 1987.

[14]Lakshminaryana, B., Zhang, J., and Murthy, K. N. S.,"The Effects of Tip Clearance on Flow Field and Losses in a Compressor Rotor," *Zeitschrift für Flugwissenschaften und Weltraumforschung*, Vol. 14, No. 4, 1990, pp. 273–281.

[15]Prato, J., and Lakshminarayana, B., "Investigation of Compressor Rotor Wake Structure at Peak Pressure Rise Coefficient and Effects of Loading," *Journal of Turbomachinery*, Vol. 115, No. 3, 1993, pp. 487–500.

[16]Lakshminaryayna, B., Zaccaria, M., and Marathe, B., "The Structure of Tip Clearance Flow in Axial Flow Compressors," *Journal of Turbomachinery*, Vol. 117, No. 3, 1995, pp. 336–347.

[17]Inoue, M., Kuroumaru, M., and Fukuhara, M., "Behavior of Tip-Leakage Flow Behind an Axial Compressor Rotor," *Journal of Engineering for Gas Turbines and Power*, Vol. 108, No. 1, 1986, pp. 7–14.

[18]Inoue, M., and Kuroumaru, M., "Structure of a Tip Clearance Flow in an Isolated Axial Compressor Rotor," American Society of Mechanical Engineers, Paper 88-GT-251, 1988.

[19]Stauter, R. C., "Measurements of the Three-Dimensional Tip Region Flow Field in an Axial Compressor," *Journal of Turbomachinery*, Vol. 115, No. 3, 1993, pp. 468–475.

[20]Goto, A., "Three-Dimensional Flow and Mixing in an Axial Flow Compressor with Different Rotor Tip Clearances," *Journal of Turbomachinery*, Vol. 114, No. 3, 1992, pp. 675–685.

[21]Puddu, P., "Tip Leakage Flow Characteristics Downstream of an Axial Flow Fan," American Society of Mechanical Engineers, Paper 96-GT-508, 1996.

[22]Foley, A. C., and Ivey, P. C., "3D Laser Transit Measurements of the Tip Clearance Vortex in a Compressor Rotor Blade Row," American Society of Mechanical Engineers, Paper 96-GT-506, 1996.

[23]Ivey, P. C., and Swoboda, M., "Leakage Effects in the Rotor Tip-Clearance Region of a Multistage Axial Compressor, Part 1: Innovative Experiments," American Society of Mechanical Engineers, Paper 98-GT-591, 1998.

[24]Rains, D. A., "Tip Clearance Flows in Axial Compressors and Pumps," Ph.D. Dissertation, California Inst. of Technology, Pasadena, CA, 1954.

[25]Zierke, W. C., Farrell, K. J., and Straka, W. A., "Measurements of the Tip Clearance Flow for a High Reynolds Number Axial Flow Rotor: Part 1—Flow Visualization, Part 2—Detailed Flow Measurements," American Society of Mechanical Engineers, Papers 94-GT-453 and 454, 1994; also *Journal of Turbomachinery*, Vol. 117, No. 4, 1994, pp. 522–532.

[26]Straka, W. A., and Farrell, K. J., "The Effect of Spatial Wandering on Experimental Laser Velocimeter Measurements of the Endwall Vortices in an Axial Flow Pump," *Experiments in Fluids*, Vol. 13, No. 2–3, 1992, pp. 163–170.

[27]Farrell, K. J., and Billet, M. L., "A Correlation of Tip Leakage Vortex Cavitation in Axial-Flow Pumps," *Journal of Fluids Engineering*, Vol. 116, No. 3, 1994, pp. 551–557.

[28]Zierke, W. C., Straka, W. A., and Taylor, P. D., "An Experimental Investigation of the Flow Through an Axial Flow Pump" (Data Bank Contribution), *Journal of Fluids Engineering*, Vol. 117, No. 3, 1995, pp. 485–490.

[29]Zierke, W. C., and Straka, W. A., "Flow Visualization and the Three-Dimensional Flow in an Axial Flow Pump," *Journal of Propulsion and Power*, Vol. 12, No. 2, 1996, pp. 250–259.

[30]Kang, S., and Hirsch, C., "Experimental Study of the Three-Dimensional Flow Within a Compressor Cascade with Tip Clearance: Part 1—Velocity and Pressure Fields," *Journal of Turbomachinery*, Vol. 115, No. 3, 1993, pp. 435–443.

[31]Kang, S., and Hirsch, C., "Experimental Study of the Three-Dimensional Flow Within a Compressor Cascade with Tip Clearance: Part 2—The Tip-Leakage Vortex," *Journal of Turbomachinery*, Vol. 115, No. 3, 1993, pp. 444–452.

[32]Kang, S., and Hirsch, C., "Tip Leakage Flow in a Linear Compressor Cascade," *Journal of Turbomachinery*, Vol. 116, No. 4, 1994, pp. 657–664.

[33]Storer, J. A., "The Interaction Between Tip Clearance Flow and the Passage Flowfield in an Axial Compressor Cascade," *9th International Symposium on Air Breathing Engines*, AIAA, Washington, DC, 1989, pp. 245–253.

[34]Storer, J. A., and Cumpsty, N. A., "Tip Leakage Flow in Axial Compressors," *Journal of Turbomachinery*, Vol. 113, No. 2, 1991, pp. 252–259.

[35]Storer, J. A., and Barton, J. P., "An Investigation of the Flow Within the Clearance Space of a Compressor Blade Tip," International Symposium of Air Breathing Engines, ISABE 91-7013, 1991.

[36]Muthanna, C., "Flowfield Downstream of a Compressor Cascade with Tip Leakage," M.S. Thesis, Dept. of Aerospace and Ocean Engineering, Virginia Polytechnic Inst. and State Univ., Blacksburg, VA, Nov. 1998, URL: http://scholar.lib.vt.edu/theses/available/etd-110798-235327/ [cited 20 Nov. 1998].

[37]Wang, Y., and Devenport, W. J., "Wake of a Compressor Cascade with Tip Gap, Part 2: Effects of Endwall Motion," *AIAA Journal*, Vol. 42, No. 11, 2004, pp. 2332–2340.

[38]Wenger, C. W., Devenport, W. J., Wittmer, K. S., and Muthanna, C., "Wake of a Compressor Cascade with Tip Gap, Part 3: Two-Point Statistics," *AIAA Journal*, Vol. 42, No. 11, 2004, pp. 2341–2346.

[39]Muthanna, C., "Effects of Free Stream Turbulence on the Flow Through a Compressor Cascade," Ph.D. Dissertation, Dept. of Aerospace and Ocean Engineering, Virginia Polytechnic Inst. and State Univ., Blacksburg, VA, May 2002, URL: http://scholar.lib.vt.edu/theses/available/etd-08222002-194441/ [cited 22 Aug. 2002].

[‡]Data available online at http://www.aoe.vt.edu/flowdata [cited 1 Oct. 2004].

[40]Wisler, D. C., "Core Compressor Exit Stage Design. Volume I—Blading Design," NASA CR-135391, Dec. 1977.
[41]Wisler, D. C., "Core Compressor Exit Stage Design. Volume IV—Data and Performance Report for the Best Stage Configuration," NASA CR-165357, April 1981.
[42]Moore, J., Moore, J. G., and Liu, B.,"CFD Computations to Aid Noise Research, Progress Rept. 2/96-10/96," Dept. of Mechanical Engineering, Virginia Polytechnic Inst. and State Univ., Blacksburg, VA, 1996.
[43]Shin, S., Ragab, S. A., and Devenport, W. J., "Numerical Simulation of Highly Staggered Cascade Flow Using an Unstructured Grid," AIAA Paper 99-3713, June–July 1999.
[44]Shin, S., "Reynolds-Averaged Navier–Stokes Computation of Tip Clearance Flow in a Compressor Cascade Using an Unstructured Grid," Ph.D. Dissertation, Dept. of Aerospace and Ocean Engineering, Virginia Polytechnic Inst. and State Univ., Blacksburg, VA, 2001, URL: http://scholar.lib.vt.edu/theses/available/etd-09122001-174121/ [cited 12 Sept. 2001].
[45]Wittmer, K. S., Devenport, W. J., and Zsoldos, J. S., "A Four Sensor Hot Wire Probe System for Three Component Velocity Measurements," *Experiments in Fluids*, Vol. 24, No. 5–6, 1998, pp. 416–423; Errata, Vol. 27, No. 4, 1999, p. U1.
[46]Bearman, P. W., "Corrections for the Effect of Ambient Temperature Drift on Hot-Wire Measurements in Incompressible Flow," *DISA Information*, Vol. 11, 1971.
[47]Kline, S. J., and McClintock, F. A., "Describing Uncertainties in Single Sample Experiments," *Mechanical Engineering*, Vol. 75, No. 1, 1953, p. 3.
[48]Mayer, E. W., and Powell, K. G., "Similarity Solutions for Viscous Vortex Cores," *Journal of Fluid Mechanics*, Vol. 238, 1992, pp. 487–507.
[49]Ragab, S. A., "Direct Numerical Simulation of Instability Waves in a Trailing Vortex," AIAA Paper 95-0591, Jan. 1995.
[50]Wittmer, K. S., and Devenport, W. J., "Effects of Perpendicular Blade–Vortex Interaction, Part 1: Turbulence Structure and Development," *AIAA Journal*, Vol. 37, No. 7, 1999, pp. 805–812.
[51]Wygnanski, I., Champagne, L., and Marasli, B., "On the Large-Scale Structures in Two-Dimensional Small-Deficit, Turbulent Wakes," *Journal of Fluid Mechanics*, Vol. 168, 1986, pp. 31–71.
[52]Moser, R. D., Rogers, M. M., and Ewing, D. W., "Self-Similarity of Time-Evolving Plane Wakes," *Journal of Fluid Mechanics*, Vol. 367, 1998, pp. 255–289.

R. So
Associate Editor